



UNIVERSITÀ
DEGLI STUDI
FIRENZE

FLORE

Repository istituzionale dell'Università degli Studi di Firenze

Unraveling Surface Basicity and Bulk Morphology Relationship on Covalent Triazine Frameworks with Unique Catalytic and Gas

Questa è la Versione finale referata (Post print/Accepted manuscript) della seguente pubblicazione:

Original Citation:

Unraveling Surface Basicity and Bulk Morphology Relationship on Covalent Triazine Frameworks with Unique Catalytic and Gas Adsorption Properties / Tuci, Giulia; Pilaski, Moritz; Ba, Housseinou; Rossin, Andrea; Luconi, Lapo; Caporali, Stefano; Pham-Huu, Cuong; Palkovits, Regina; Giambastiani, Giuliano. - In: ADVANCED FUNCTIONAL MATERIALS. - ISSN 1616-301X. - STAMPA. - 27:(2017), pp. 1605672-1605672.

Availability:

The webpage <https://hdl.handle.net/2158/1085744> of the repository was last updated on 2021-03-30T11:37:05Z

Published version:

DOI: 10.1002/adfm.201605672

Terms of use:

Open Access

La pubblicazione è resa disponibile sotto le norme e i termini della licenza di deposito, secondo quanto stabilito dalla Policy per l'accesso aperto dell'Università degli Studi di Firenze (<https://www.sba.unifi.it/upload/policy-oa-2016-1.pdf>)

Publisher copyright claim:

Conformità alle politiche dell'editore / Compliance to publisher's policies

Questa versione della pubblicazione è conforme a quanto richiesto dalle politiche dell'editore in materia di copyright.

This version of the publication conforms to the publisher's copyright policies.

La data sopra indicata si riferisce all'ultimo aggiornamento della scheda del Repository FloRe - The above-mentioned date refers to the last update of the record in the Institutional Repository FloRe

(Article begins on next page)

Aziridine Functionalized Multi-Walled Carbon Nanotubes: a Robust and Versatile Catalyst for the Oxygen Reduction and Knoevenagel Condensation†

Giulia Tuci,[§] Lapo Luconi,[§] Andrea Rossin,[§] Enrico Berretti,^ξ Housseinou Ba,^φ Massimo Innocenti,^ξ

Dmitry Yakhvarov,^ψ Stefano Caporali,^ξ Cuong Pham-Huu^φ and Giuliano Giambastiani^{§,ψ,*}

[§] Institute of Chemistry of OrganoMetallic Compounds, ICCOM-CNR and Consorzio INSTM, Via Madonna del Piano, 10 – 50019, Sesto F.no, Florence, Italy. Email: giuliano.giambastiani@iccom.cnr.it

^ξ Department of Chemistry, University of Florence, 50019 Sesto F.no, Florence, Italy

^φ Institut de Chimie et procédés pour l'Energie, l'Environnement et la Santé(ICPEES), UMR 7515 CNRS - Université de Strasbourg, Strasbourg, France

^ψ Kazan Federal University, 420008 Kazan, Russian Federation.

KEYWORDS

Chemical functionalization; Multi-walled carbon nanotubes; N-decoration; Knoevenagel condensation; Oxygen reduction reaction; electrocatalysis

ABSTRACT

This paper describes the exohedral N-decoration of multi-walled carbon nanotubes (MWCNTs) with NH-aziridine groups via [2+1] cycloaddition of a *tert*-butyl-oxycarbonyl nitrene followed by controlled thermal decomposition of the cyclization product. The chemical grafting with N-containing groups deeply modifies the properties of the starting MWCNTs, generating new surface microenvironments with specific base (Brønsted) and electronic properties. Both these features translate into a highly versatile single-phase heterogeneous catalyst (**MW@N^{Az}**) with remarkable chemical and electrochemical performance. Its surface base character promotes the Knoevenagel condensation with superior activity to that of related N-doped and N-decorated carbon nanomaterials of the *state-of-the-art*; the N-induced electronic surface redistribution drives the generation of high energy surface “C” sites suitable for O₂ activation and its subsequent electrochemical reduction (ORR).

1. Introduction

Nitrogen-containing carbon nanomaterials (N-CNMs) represent green and sustainable catalysts alternative to classical metal-based systems for a number of industrially relevant transformations.¹⁻⁴ Since the pioneering works by Gong⁵ and Wang,⁶ several studies have demonstrated their versatility in a wide range of processes: from renewable energy production and storage to the manufacturing of commodities and feedstocks. The inclusion of nitrogen in the sp^2 carbon structure of mono- or bi-dimensional materials induces a significant change of their chemico-physical and morphological properties. In particular, the in-depth alteration of the electronic density distribution within N-doped systems (compared to their undoped counterparts) along with the basic character of their outer surface (due to the presence of exposed N-sites) have remarkable influence on their catalytic performance.^{1-4, 7} In addition, the absence of metallic active sites definitively prevents some common catalyst deactivation phenomena (*i.e.* metal leaching, passivation/poisoning and sintering) that largely affect the efficiency of classical metal-based heterogeneous systems engaged in liquid- or gas-phase processes.

The electron-rich surface of N-CNMs has been shown to be very promising for electrochemical applications.^{8, 9} In fact, a wide variety of N-CNMs have been employed for O_2 reduction (ORR) in fuel cell devices^{2, 5, 6, 10-12} as well as for the electrochemical conversion of more challenging small molecules like CO_2 into products and reduction intermediates of added value.^{13, 14} Nanomaterials with a N-rich outer surface¹⁵ in combination with high specific surface area (SSA) and electrical conductivity constitute a class of single-phase systems featured by unique electrochemical performance. The inclusion of nitrogen(s) in the Csp^2 network breaks the material electroneutrality and determines a net redistribution of the charge density at the neighboring carbon sites,¹⁶ thus improving the material oxygen adsorption properties and facilitating the occurrence of the electrochemical oxygen reduction.^{17, 18} An appropriate balance between a moderate oxygen binding energy and a highly localized electron density around the active site seems to be crucial for getting highly performing ORR catalysts.^{5, 19} Recent findings from our group have demonstrated how a tight control of the surface properties of carbon-based nanomaterials is conveniently achieved by chemical functionalization of their outer surface with tailored N-containing heterocycles.^{11, 12} The chemical approach allows for a fine control of N-dopants in terms of N-configuration and electronic charge distribution at the heterocycles and it offers a unique tool to the in-depth comprehension on the role of specific N-functionalities²⁰ in O_2 activation.

Surface basicity is another fundamental prerequisite for the exploitation of these solid base catalysts in industrial key transformations. Studies in recent years have demonstrated the ability of N-CNMs to act as effective base catalysts to promote the Knoevenagel condensation,²¹ a C-C bond forming reaction between carbon acid reagents and aldehydes or ketones to give α,β -unsaturated compounds

useful in fine-chemical industrial synthesis.^{22, 23} Since the pioneering work by Van Dommele *et al.*,²⁴ N-doped carbon nanotube samples with variable basicity²⁵ have been synthesized by Chemical Vapor Deposition (CVD) and employed as effective and reusable heterogeneous systems for promoting the above mentioned condensation process. On this ground, other synthetic methods aimed at preparing N-CNMs with increased surface basicity have been developed. Graphitic carbon nitrides,²⁶⁻³² ammoxidated commercial carbon sources³³ or CN_x derivatives,³⁴ N-rich graphene oxides (N-GO)³⁵ and amino-decorated fullerenes³⁶ are among the most representative examples of heterogeneous systems employed with success for the Knoevenagel process as well as for other base-driven transformations.³⁷

This paper describes the chemical functionalization of MWCNTs with aziridine groups and their versatile application as effective and re-usable solid base systems for the Knoevenagel condensation and the electrochemical oxygen reduction reaction. The common thread that links aziridine functionalized MWCNTs with these catalytic technologies lies on the control of the material surface properties (basic and electronic) exerted by the exposed N-sites. While their Brønsted basic character is the essential prerequisite for these solid systems to be effectively engaged in the Knoevenagel condensation, the surface electronic redistribution caused by the exohedral N-doping generates "C" sites suitable for O₂ activation and the subsequent O=O bond breaking under electrochemical conditions.

2. Experimental

2.1 General Considerations

All manipulations dealing with the chemical functionalization of MWCNT were carried out under dry nitrogen atmosphere using standard Schlenk-type techniques. Nitrogen (>99.999%; Rivoira) was dried through a CaCl₂ column and deoxygenated with an oxysorb cartridge from Messer Griesheim prior to use. *o*DCB (*o*-dichlorobenzene), EtOH, *i*PrOH, *n*BuOH and thf were dried according to the literature procedures³⁸ and stored under nitrogen atmosphere. Dry acetonitrile (CH₃CN) and toluene were obtained by means of an MBraun Solvent Purification System. MWCNTs (98% in C) were purchased from Sigma-Aldrich (lot. no. MKBH5814 V) and used as received. *tert*-Butyl azidoformate was prepared in a multigram scale according to literature procedures.³⁹ Unless otherwise stated, all other chemicals were purchased from commercial suppliers and used as received without further purification.

2.2 Functionalization of MWCNTs with *tert*-butyl azidoformate: synthesis of MW@N^{BOC}. In a 250 mL three-necked flask equipped with a magnetic stir bar and a reflux condenser, 60 mg of MWCNTs were suspended in 100 mL of dry and degassed *o*DCB. The suspension was sonicated for 30 minutes and then heated to 160 °C. The *tert*-butyl azidoformate (1 g) was added dropwise under stirring and the temperature was maintained at 160 °C for 45 min. The suspension was then cooled to room temperature, diluted with ethyl acetate (40 mL), sonicated for 10 minutes and centrifuged in order to recover the solid material. The solid residue underwent purification via three successive sonication/centrifugation/washing cycles with ethyl acetate and dichloromethane (1 x AcOEt, 2 x CH₂Cl₂) before being suspended in dichloromethane, sonicated for 15 minutes and filtered through a 0.2 µm-pore membrane (PTFE supported Whatman™) filter. The recovered MW@N^{BOC} was finally dried under vacuum at 50 °C to constant weight.

2.3 Synthesis of MW@N^{Az} by controlled thermal treatment of MW@N^{BOC}. 200 mg of MW@N^{BOC} were placed in a quartz tube and heated at 250 °C (heating rate: 10 °C/min) for 12 h under dynamic ultra-high vacuum. MW@N^{Az} was then recovered and stored at room temperature under nitrogen atmosphere. The prolonged exposure of MW@N^{Az} to air causes a progressive carbonation of the surface exposed basic N-sites.

2.4 Catalyst characterization and analysis conditions

Thermogravimetric Analysis (TGA-MS). Analyses were performed under either N₂ atmosphere (50 mL/min) or air (100 mL/min) on an EXSTAR Thermo Gravimetric Analyzer (TG/DTA) Seiko 6200 coupled with a ThermoStar GSD 301T (TGA-MS) for MS analysis of volatile compounds. *X-ray Photoelectron Spectroscopy (XPS).* Analyses were performed in an ultra-high vacuum system (10⁻⁹ mbar) equipped with a VSW HAC 5000 hemispherical electron energy analyzer and a non-monochromatized Mg-Kα X-ray source (1253.6 eV). The source power was 120 W (12 kV x 10 mA) and the spectra were acquired at 53° takeoff angle respect to the sample normal. Survey spectra were acquired at a pass energy of 44 eV with an energy step size of 1 eV. High resolution spectra of detected elements were recorded for quantitative and detailed BE chemical shift analysis at a pass energy of 22 eV with a step size of 0.05 eV. In the set conditions the overall energy resolution was 1.0 eV measured as a full-width at half maximum (FWHM) of the Ag 3d_{5/2} line of a pure silver reference. Samples, in the form of powders, were fixed on vacuum compatible carbon adhesive tape ensuring, as much as possible, a uniform coverage and were kept in the introduction chamber for at least 12 h, allowing the removal of adsorbed volatile substances. No charge compensation was used and the spectra were corrected using the sp² graphitic component of the C 1s spectrum as internal reference (binding energy, BE = 284.6 eV). Elemental semi quantitative atomic percentages were

calculated by fitting the spectra with mixed Gaussian–Lorentzian peaks after removal of a Shirley-type background and applying tabulated sensitivity factors.⁴⁰ *Transmission Electron Microscopy (TEM)*. Analyses were performed by a Philips CM12 microscope operating at 120 kV, on samples prepared by drop-casting previously sonicated suspensions (EtOH) over copper grids coated with a Formvar film (FF200-Cu-Formvar film only). TEM images were recorded with a CCD camera (Gatan 791). *Elemental analyses* were performed using a Thermo FlashEA 1112 Series CHNS-O elemental analyzer, and elemental average values were calculated over three independent runs. *Acid-Base Titration* of pristine and **MW@N^{Az}** samples. Five milligrams of the N-decorated material were suspended in 7 mL of a standard HCl solution (2.8×10^{-3} M, standardized with Na₂CO₃ as primary standard), sonicated for 30 min, and maintained in the dark at rt under stirring for 48 h. Afterward the suspension was centrifuged, and three aliquots of the supernatant solution were titrated with a standardized solution of NaOH (2×10^{-3} M). The N-basic sites content (N %) was calculated for each sample as the average value over three independent runs.^{41, 42} *GC-MS* analyses were performed on a Shimadzu QP2010S apparatus equipped with a flame ionization detector and a Supelco SPB-1 fused-silica capillary column (30 m length, 0.25 mm i.d., 0.25 μ m film thickness).

2.5 Catalytic runs

2.5.1 Knoevenagel condensation reaction. In a typical procedure, 10-20 mg of **MW@N^{Az}** are suspended in 3 mL of the dry and degassed solvent of choice (Table 1) and sonicated (10-15 min.) to get a homogeneous catalyst suspension. Afterwards, 2 mmol of the electrophile (**1a-g**) and 2.1 mmol (1.05 eq.) of the nucleophile (**2-3**) are added in sequence and the reaction is heated in the dark to its final temperature and maintained under moderate stirring for the desired reaction time. The reaction mixture is then cooled in an ice bath and treated under stirring with 2 mmol of an internal standard (1-dodecene for the reactions of **1a-f** with **2** and **3**; *trans,trans*-dibenzylideneacetone for the reaction of **1g** with **2**). After catalyst filtration through a 0.2 μ m-pore membrane (PTFE supported WhatmanTM), the clear solution was analyzed by GC-MS. For catalyst recycling tests, **MW@N^{Az}** was decanted from the mother liquor upon centrifugation and carefully washed/sonicated twice with freshly distilled EtOH before being rinsed with an EtOH solution of reagents.

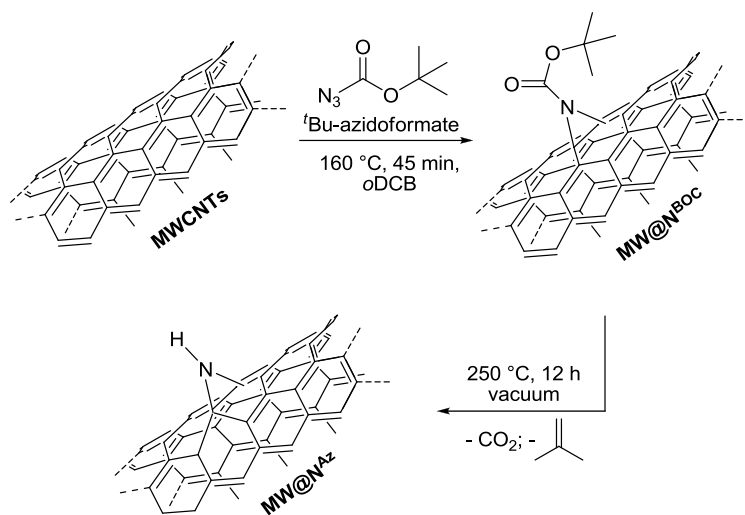
2.5.2 Electrochemical oxygen reduction reaction (ORR) with **MW@N^{Az}; materials and analysis conditions.** *Rotating-Ring Disk Electrode (RRDE)* measurements were performed using a ring-disk electrode from Pine Instrument Co. consisting of a glassy carbon (GC) disk insert (\varnothing 5 mm; $A = 0.196$ cm²) and a Pt ring ($A = 0.11$ cm²). All electrochemical measurements were carried out using an Autolab bi-potentiostat/galvanostat in a single compartment glass cell using a three-electrode

arrangement. The working electrode was prepared as follows: a proper amount of CNTs (10 mg of MWCNTs or **MW@N^{Az}**) was dispersed in 0.220 g of water, 0.112 g of ethanol, and 0.084 g of a Nafion solution (5 wt % in lower aliphatic alcohols and water). The resulting ink was sonicated for 30-45 min and drop-casted onto the glassy carbon electrode (see Table S1). The as-prepared electrode was then dried at room temperature. A platinum wire was used as counter electrode, and a double junction Ag/AgCl/KCl sat. electrode served as reference electrode. All RRDE experiments were recorded at a scan rate of 5 mV/s in the potential range from -1.1 to 0.2 V vs. Ag/AgCl/KCl sat. Nitrogen or oxygen was used to purge the solution to achieve an oxygen-free or an oxygen-saturated electrolyte solution, respectively. Commercial Metrohm Pt electrode (\varnothing 3 mm) was used for comparison, and all measurements were repeated at least four times. Finally, the measurement setup, the moderate electrolyte viscosity and the entity of the measured currents did not require any ohmic compensation. All prepared CNT inks were indefinitely stable in air for months with neither any apparent decomposition nor alteration of their electrochemical performance. The number of electrons transferred per O₂ molecule (*n*) in the ORR for the different catalysts has been calculated by the Koutecky–Levich equation applied to the ORR curves recorded at different electrode spin rates (rpm)⁴³ and confirmed from the Pt-ring currents recorded at the RRDE electrode. For the electrochemical data processing see ESI†.

3. Results and Discussion

3.1 Covalent exohedral functionalization of MWCNTs with aziridine groups (**MW@N^{Az}**)

The adopted procedure for the N-decoration is based on a two-step protocol that includes a nitrene [2+1] cycloaddition⁴⁴ to the π -electron system of MWCNTs⁴⁵⁻⁴⁸ followed by a controlled thermal decomposition of the reaction product.⁴⁹ The cycloaddition reaction is performed under relatively mild conditions starting from pristine MWCNTs and the freshly prepared *tert*-butyl-azidoformate.³⁹ The *tert*-butyloxycarbonylaziridino-MWCNTs (**MW@N^{BOC}**) intermediate undergoes a thermal treatment under ultra-high vacuum that readily and selectively decomposes the carbamate units into isobutene and CO₂ and leads to the target aziridine-NH functionalized sample (**MW@N^{Az}**) (Scheme 1).⁴⁹ At odds with other covalent functionalization protocols where basic N-containing groups can be grafted to the surface of complex carbon structures as dangling arms,^{11, 12} the [2+1] nitrenes cycloaddition guarantees a more intimate connection between the exohedral N-dopant and the sp² carbon network.



Scheme 1. Sidewall functionalization by [2+1] cycloaddition of **1** followed by controlled thermal decomposition of the **MW@N^{BOC}** intermediate to give **MW@N^{Az}**.

The **MW@N^{BOC}** intermediate undergoes a careful work-up treatment consisting in successive and multiple sonication/centrifugation and filtration cycles to remove solvent (1,2-Dichlorobenzene, *o*DCB) and the excess of starting reagent. Aziridine nuclei present a relatively high thermal stability; the decomposition of **MW@N^{BOC}** occurs selectively with evolution of volatile side-products that do not bring about any organic contamination of the final material. Finally, the target **MW@N^{Az}** sample is isolated without any (acid-base) work-up treatment, thus excluding the occurrence of further “chemical” alterations of the nanomaterial surface.²⁰

The as-prepared **MW@N^{Az}** sample has been spectroscopically (XPS) and morphologically (TEM) characterized. TEM images (Fig. S1, see ESI†) of **MW@N^{Az}** do not reveal any appreciable morphological alteration in terms of tube length and diameter compared to the pristine sample (MWCNTs). XPS spectra of the functionalized MWCNTs before (**MW@N^{BOC}**) and after (**MW@N^{Az}**) the thermal phase show characteristic N 1s profiles consistent with one main component at 400.3 and 399.1 eV, typical of carbamate⁵⁰ and aziridine⁵¹ units, respectively (Fig. 1A). A minor shoulder at higher binding energies (400.8 eV) in the N 1s profile of **MW@N^{Az}** is ascribed to the spontaneous partial amine carbonation upon material exposure to air.^{51, 52}

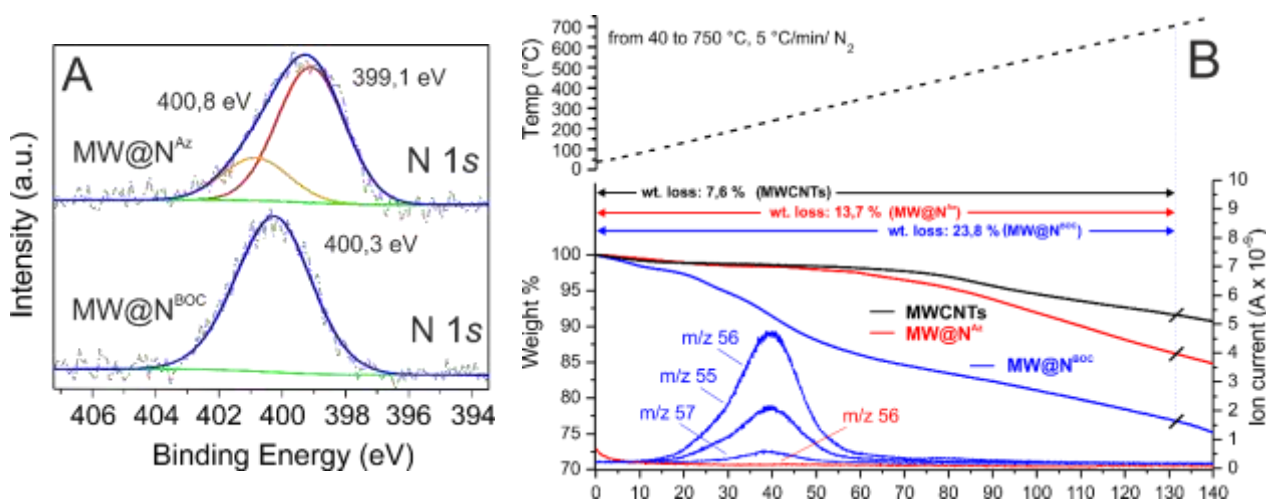


Fig 1. A) XPS high resolution N 1s core level regions and related fits of **MW@N^{Az}** (top) and **MW@N^{BOC}** (bottom). B) TGA profiles of MWCNTs (—), **MW@N^{Az}** (—) and **MW@N^{BOC}** (—) intermediate in the 40-750 °C temperature range. MS analyses of selected volatiles are reported for **MW@N^{Az}** (—) and **MW@N^{BOC}** (—) (bottom lines). Weight loss % are measured in the 40-700 °C temp. range.

Evidence of the occurred functionalization is given by comparative TGA-MS analyses of **MW@N^{BOC}**, **MW@N^{Az}** and pristine MWCNTs. As Fig. 1B shows, **MW@N^{BOC}** presents a marked weight loss of 16.2 % in the 40-700 °C temperature range (calculated as the weight loss difference with MWCNTs in the same temperature range). A mass analysis of the low molecular weight volatiles (from 25 to 125 a.m.u.) reveals the thermal decomposition and rearrangement of the *tert*-butoxyl groups of **MW@N^{BOC}** below 300 °C with the concomitant isobutene evolution (m/z 56 [M^+]; m/z 55 [M^+-1]; m/z 57 [M^++1]; Fig. 1B, — bottom lines). The thermal treatment that quantitatively converts **MW@N^{BOC}** into **MW@N^{Az}** (Scheme 1) decomposes the labile carbamate groups while preserving the overall N-content at the material surface (*vide infra* elemental analysis - EA and acid-base titration). Consequently, the TG of **MW@N^{Az}** shows a more stable TG profile compared to **MW@N^{BOC}** and MS peaks due to the decomposition/rearrangement of *tert*-butoxyl groups disappear (Fig. 1B, — bottom line). A quantitative N-loading is roughly established by CHN elemental analysis on all functionalized samples and refined *via* acid-base titration^{12, 41, 42} for the base **MW@N^{Az}** sample only (Table 1); hence it can be inferred that about 0.71 mmol/g of aziridine groups are covalently tethered to the nanotube sidewalls.

	Elemental analysis ^a		N(%) acid-base titration ^a	N-groups mmol/g
	C(%)	N(%)		
MWCNTs	98.6	-	-	-
MW@N ^{BOC}	91.6	1.1	n.d.	0.79
MW@N ^{Az}	94.1	0.9	1.1	0.71

Table 1. Elemental analyses for **MW@N^{BOC}**, **MW@N^{Az}** and pristine MWCNTs. ^a C% and N% contents (including N% *via* acid-base titration) are calculated as average values over three independent runs.

3.2 Knoevenagel condensation with aziridine decorated MWCNTs (MW@N^{Az})

For the Knoevenagel condensation promoted by the MW@N^{Az} catalyst, benzaldehyde (**1a**) as electrophile and two acid carbons - ethyl cyanoacetate (**2**) and dimethyl malonate (**3**) - as nucleophiles are selected as model reagents. The reactions proceed smoothly in EtOH with a markedly low catalyst loading (from 10 to 20 mg of MW@N^{Az}) to give condensation products **4a** and **5a** in 86% and 42% respectively after 5h at reflux of solvent (Table 2, entries 1 and 8). Prolonged reaction times increased the chemical conversions (> 99% for **4a** and 49% for **5a**) without any appreciable reagents degradation or by-products formation. Attempts to boost the chemical yield of **5a** by increasing the reaction time and temperature led to the appearance of undesired benzaldehyde side-products. As Table 2 shows, polar protic solvents (*i.e.* EtOH and *i*PrOH) afford the best catalytic outcomes (Table 2, entries 1 and 3 *vs.* 4 and 5). This result is reasonably ascribed to the homogeneous and stable dispersion of the nanomaterial in the polar protic reaction medium. On the other hand, thf and toluene (in particular) cause severe catalyst segregation phenomena; carbon nanotube aggregates are formed and readily separate off from the reaction mixture (Table 2, entries 1-5). Catalyst's turn over number (TON) is calculated for each run as mmol of **1a** converted *per* g of catalyst ($\text{mmol}_{\text{conv.}} \cdot \text{g}_{\text{cat}}^{-1}$); it offers a useful clue to debate on the effectiveness of MW@N^{Az} in the Knoevenagel process compared to other N-doped systems of the *state-of-the-art*.⁵³ TON values measured for MW@N^{Az} to afford **4a** are markedly higher than those calculated from the literature for related N-CNM catalysts; in the condensation of **1a** with **2**, TON of MW@N^{Az} is over five times higher than that reported for alkyl-amino decorated fullerenes as catalyst.³⁶ In addition, the robustness of MW@N^{Az} as solid base catalyst for the Knoevenagel condensation is witnessed by its easy recovery and reuse in the condensation process without any significant alteration of its original catalytic performance even after several runs (Table 2, entries 6 and 7). After each run, the catalyst is decanted from the mother liquor upon centrifugation and washed twice with freshly distilled EtOH before being rinsed with an EtOH solution of reagents, sonicated till a homogeneous suspension is formed and heated to the final reaction temperature. After six catalytic cycles, it maintains its catalytic performance virtually unchanged (Table 2, entry 7 and Fig. S2A, see ESI†).

The reactions of ethyl cyanoacetate (**2**) and variably substituted benzaldehydes (**1b-e**), including an aliphatic aldehyde (**1f**) and a cyclohexanone derivative (**1g**), are finally investigated with the aim at checking the tolerance of MW@N^{Az} towards different functional groups at the electrophile and validating the general character of the catalytic process with various carbonyl compounds. 4-nitro benzaldehyde (**1b**), 2-bromo (**1c**) and 4-bromo-benzaldehyde (**1d**) and 4-methoxy benzaldehyde (**1e**) gave the respective condensation products (**4b-e**) from good to quantitative yields after 5h stirring at the reflux of EtOH (Table 3, entries 1, 4, 6 and 8). TON values were calculated for each catalytic run

at partial substrate conversions (Table 3, entries 2, 5, 7 and 8) as obtained for **1b-d** and **1e** after 3h and 5h, respectively.

Table 2. Catalytic activity of **MW@N^{Az}** for the Knoevenagel condensation of benzaldehyde (**1a**) with selected C-nucleophiles (**2**, **3**).^a

1a **2**; R = CO₂Et; R' = CN
3; R = R' = CO₂Me **4a**; R = CO₂Et; R' = R' = CN
5a; R = R' = CO₂Me

Entry	Nucl.	Solvent	Product	Yield (%) ^b	TON (mmol _{conv.} g _{cat.} ⁻¹)
1	2	EtOH	4a	86	172
2 ^c	2	EtOH	4a	> 99	-
3	2	ⁱ PrOH	4a	82	164
4	2	toluene	4a	14	28
5 ^d	2	thf	4a	6	12
6 ^e	2	EtOH	4a	79	158
7 ^f	2	EtOH	4a	81	162
8 ^g	3	EtOH	5a	42	42
9 ^{g,c}	3	EtOH	5a	49	49

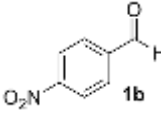
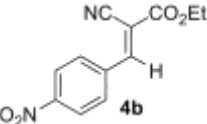
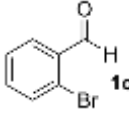
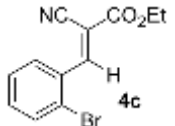
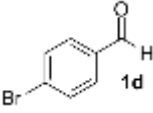
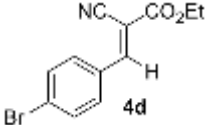
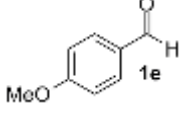
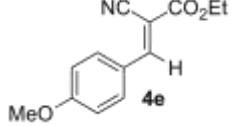
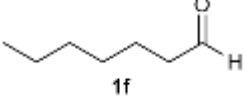
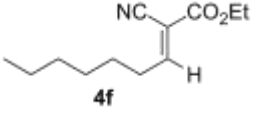
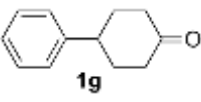
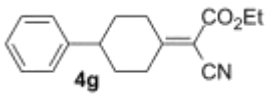
^a Reaction conditions: **MW@N^{Az}** cat. (10 mg – otherwise stated), aldehyde (**1a**; 2.0 mmol), nucleophile (**2**, **3**; 2.1 mmol, 1.05 eq); Reaction time: 5h at 78°C (otherwise stated) ^b Calculated from GC-MS using 1-dodecene as internal standard. ^c Reaction time: 7h. ^d Reaction temperature: 66°C. ^e Recycled catalyst – 3rd run. ^f Recycled catalyst – 6th run. ^g **MW@N^{Az}** cat. (20 mg)

Under the same conditions (5h in refluxing EtOH) the aliphatic aldehyde (**1f**) gave **4f** with 74% yield while a complete conversion was achieved by doubling the reaction time (Table 3, entry 10). For all scrutinized issues, the catalyst showed remarkable tolerance to functional groups at the electrophile and excellent conversions (Table 3). The condensation with ketone **1g** gave only moderate reaction yield (Table 3, entry 11). A significant improvement was obtained by doubling the catalyst loading and increasing the reaction time and temperature (Table 3, entries, 12-13); **4g** was isolated in 57% yield using 20 mg of **MW@N^{Az}** at reflux of ⁿBuOH for 16h. In spite of the harsh reaction conditions, the reaction course didn't show any apparent reagents degradation or side-products formation.

The overall N-content at the outer material surface along with its basic character (typical of secondary amines) is responsible of the markedly high catalytic activity of **MW@N^{Az}** in the Knoevenagel condensation. In spite of a moderate N-surface functionalization, the outer aziridine groups improve the deaggregation of the catalytic material in polar protic solvent thus allowing to get a homogeneous CNT dispersion in the reaction medium with catalytic performance similar to those of homogeneous base systems. On the other hand, the macromolecular nature of the CNT carrier

allows its easy recovery and re-use at the end of the process while keeping its catalytic performance unchanged even after several cycles (Fig. S2B, see ESI†).

Table 3. Catalytic activity of **MW@N^{Az}** for the Knoevenagel condensation of **2** with substituted aldehydes and ketones.^a

Entry	Electr.	Product	Yield (%) ^b	TON (mmol _{conv.} g _{cat.} ⁻¹)
1			> 99	-
2 ^c	”	”	81	162
3 ^d	”	”	79	158
4			> 99	-
5 ^c	”	”	68	136
6			> 99	-
7 ^c	”	”	73	146
8			79	158
9			74	148
10 ^e	”	”	> 99	-
11			5	10
12 ^f	”	”	37	37
13 ^g	”	”	57	57

^a Reaction conditions: **MW@N^{Az}** cat. (10 mg – otherwise stated), electrophile (**1b-g**; 2.0 mmol), nucleophile (**2**; 2.1 mmol, 1.05 eq); Reaction time: 5h at 78°C (otherwise stated) ^b Calculated from GC-MS using 1-dodecene (for entries 1-10) or *trans,trans*-dibenzylideneacetone (for entries 11-13) as internal standards. ^c Reaction time: 3h. ^d Recycled catalyst – 6th run. ^e Reaction time: 10h. ^f **MW@N^{Az}** cat. (20 mg), reaction time: 16h. ^g **MW@N^{Az}** cat. (20 mg), reaction time: 16h at reflux of ⁿBuOH (118 °C).

3.3 Electrochemical tests on MW@N^{Az} as catalyst for the ORR. Taking advantage from the N-induced redistribution of the electronic charge density at the **MW@N^{Az}** surface, the same material has been exploited for O₂ activation and its subsequent electrochemical reduction. To this aim, a **MW@N^{Az}/Nafion** ink is prepared and casted on a rotating glassy carbon (GC) electrode to give a thin and homogeneous film after solvent evaporation (see Experimental Section). The as-prepared

electrocatalyst has been studied by cyclic voltammetry (CV) using a three electrode cell consisting of an Ag/AgCl/KCl saturated reference electrode and a Pt counter electrode operating in a 0.1 M KOH solution. As Fig. 2A shows, under O₂-saturated conditions **MW@N^{Az}** presents a marked and irreversible ORR cathodic peak not present under a N₂-saturated environment (red vs. blue curve). The catalyst's ink is then employed for rotating ring disk electrode (RRDE) measurements and its performance compared with those of pristine MWCNTs, bare GC, and the commercial Metrohm Pt-polycrystalline electrode (Ø 3 mm) under identical O₂-saturated alkaline conditions (Fig. 2B). The amount of **MW@N^{Az}** deposited at the RRDE electrode is fixed to 336 µg/cm² in accord with the highest number of exchanged electrons measured for electrodes prepared at variable **MW@N^{Az}** ink loadings (see also Table S1, see ESI†).

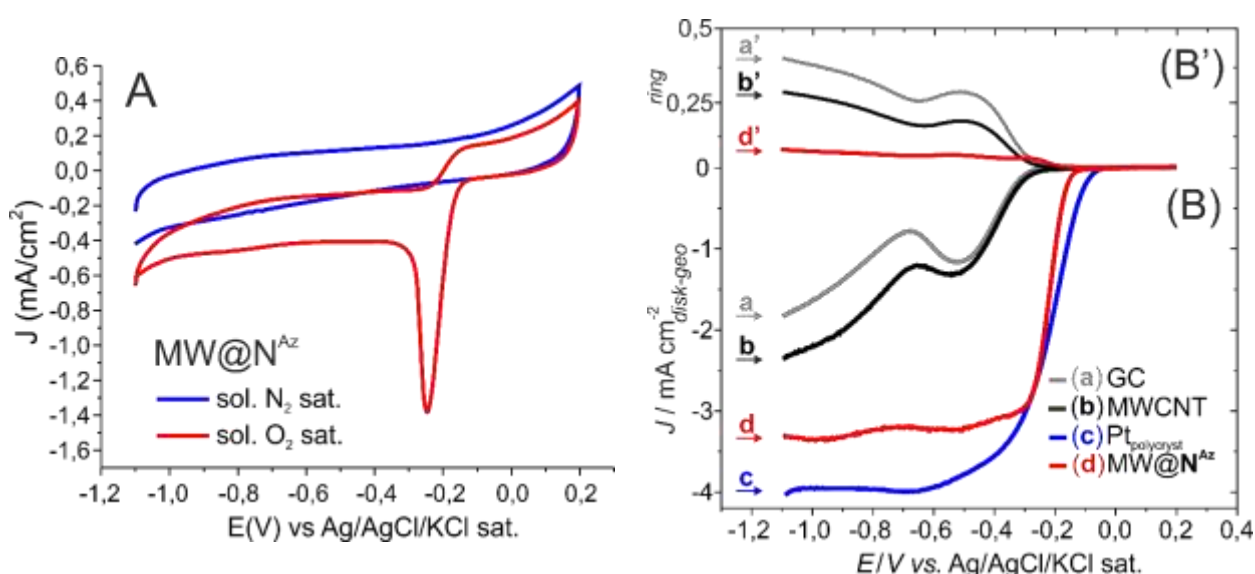


Fig. 2. (A) Cyclic voltammograms of **MW@N^{Az}** recorded under N₂-saturated (blue) and O₂-saturated solutions (red). The potential was linearly swept from -1.1 to 0.2 V at a scan rate of 5 mV s⁻¹ vs. Ag/AgCl/KCl sat. as the reference electrode. (B) RRDE current-potential curves at 293 K for ORR in O₂ saturated 0.1 M KOH solution recorded by using a rotating ring-disk GC electrode [GC disk, A = 0.196 cm²] with (B') Pt ring [A = 0.11 cm²]. All samples are measured at an angular rotation rate (ω) of 800 rpm.

Linear sweep voltammograms are recorded for each electrocatalyst at different spin rates (from 400 to 2000 rpm), while sweeping potentials linearly from -1.0 to 0.2 V and reversing them against Ag/AgCl/KCl sat. (Fig. S3, see ESI†); for all the electrochemical profiles, background currents measured under saturated N₂ conditions at the same potential scan rate (5 mV s⁻¹) are subtracted from the respective curves to eliminate all capacitive contributions. Fig. 2B shows the ORR polarization curves recorded at 800 rpm for each system, along with the respective ring current values relative to the oxidation of hydrogen peroxide ions (HO₂⁻) measured at the Pt-ring electrode held at a potential of 0.50 V (Fig. 2B'). As Fig. 2B shows, the onset potential (E_{on}) measured for **MW@N^{Az}** maintains a remarkable and positive shift compared to pristine MWCNTs (curve d vs. b) and GC (curve d vs. a). While ORR starts at -0.299 V (E_{on}) on pristine MWCNTs, corresponding to an overpotential of

ca. 200 mV compared to Pt (Table 4, entry 2 vs. 4; Fig. 2B, curve b vs. c), less than 50 mV overpotential are measured for **MW@N^{Az}** (Fig. 2B, curve d vs. c). Moreover, GC and pristine MWCNTs present a clear reduction pre-wave at low overpotentials, followed by a second reduction wave around -0.7 V, being indicative of a prevalent 2e⁻ reduction path.⁵⁴⁻⁵⁷ In line with that, a markedly lower ring current is measured for **MW@N^{Az}** (Fig. 2B') compared to pristine MWCNTs and GC. The ORR performance (number of transferred electrons per O₂ molecule - n_E) in the diffusion and kinetically limited regions (from -0.65 to -0.95 V) is evaluated for each electrocatalyst on the basis of the Koutecky-Levich (K-L) equation.^{55, 58} K-L plots of each catalytic system obtained at -0.7V are presented in Fig. S4 of the ESI material. All curves show excellent linearity, thus implying a first-order reaction toward dissolved O₂. For the sake of completeness, n_E in the same potentials region is also calculated on the basis of the Pt ring currents at the RRDE system (Fig. 2B' and Fig. S5, see ESI†) due to the H₂O₂ produced in the electrochemical processes. The final $n_{E(-0.7V)}$ for **MW@N^{Az}**, calculated as average value from the two aforementioned methods is fixed to 3.7e⁻, a value that is consistent with a prevailing 4e⁻ reduction process promoted by the metal-free catalyst. This conclusion is further supported by the rather moderate ring current measured at the Pt ring electrode with **MW@N^{Az}** as catalyst, indicative of a scarce amount of HO₂⁻ ions generated in the process (Fig. 2B' and Fig. S5, see ESI†). Onset potential values (E_{on}) measured for each catalyst along with the average number of exchanged electrons for O₂ molecule in the process are listed on Table 4 (see also the Experimental Section for calculation details).

Table 4. E_{on} values (V) and average number of electrons transferred ($n_{E=-0.7V}$) for O₂ molecule as derived from plots in Figs. 2B and 2B' and S4, respectively.

Entry	Catalyst	E_{on} (V)	$n_{E=-0.7V}^a$	$n_{E=-0.7V}^b$	$n_{E=-0.7V}^c$
1	GC	-0.307	1.9	2.6	2.3
2	MWCNTs	-0.299	2.3	3.1	2.7
3	MW@N^{Az}	-0.149	3.5	3.8	3.7
4	Pt	-0.101	3.9	-	-

^a Calculated from K-L plots. ^b Calculated from Pt ring currents (H₂O₂ %). ^c Calculated as average value from K-L and Pt ring currents measurements.

The electrochemical behavior of **MW@N^{Az}** compared to that of its unfunctionalized counterpart (MWCNTs) (Fig. 2B, curve d vs. b) unambiguously demonstrates the effective metal-free action of the N-decorated catalyst in the ORR process. Although the presence of metal residues in the bulk material (below 2 wt. % see Fig. S6, see ESI†) is a fact for both systems, the markedly improved electrochemical performance of **MW@N^{Az}** compared to MWCNTs is rationally ascribable to the material N-decoration only and, in turn, to the N-induced redistribution of the electronic charge

density at the outer material surface. Long-term cycling RRDE tests (measurements in the $-1.1 \div 0.2$ V range at 200 mV s^{-1} , 800 rpm in 0.1 M KOH at 25°C) have been finally carried out to investigate the stability of **MW@N^{Az}** under the electrochemical conditions. As Fig. S7 shows, a moderate J decrease ($< 7\%$ measured at -0.7 V) takes place after about 1000 electrochemical cycles and it asymptotically stabilizes at the steady-state conditions; this behavior indicates the high resistance of the catalyst toward deactivation under operative conditions. Finally, the tolerance of the **MW@N^{Az}** electrocatalyst to the direct exposure of methanol as poisoning agent has been investigated. Methanol tolerance is an essential prerequisite for the successful exploitation of ORR electrocatalysts at the cathode of direct methanol fuel cells (DMFC). Indeed, fuel crossover through the polymer electrolyte membrane (from the anode to the cathode side) may cause severe reduction of the overall DMFC performance.⁵⁹ Both **MW@N^{Az}** and the benchmarking 20 wt % Pt/C (Vulcan® XC-72) electrocatalysts have been treated with methanol (until a 1 M methanol concentration of the final electrolyte solution) during the ORR test (Fig. S8, see ESI†). Upon methanol addition, the **MW@N^{Az}** maintains its current response virtually unchanged, while the 20 wt % Pt/C relative current drops down remarkably due to the occurrence of the undesired methanol oxidation.^{60, 61}

4. Conclusions

In this study, aziridine decorated multi-walled carbon nanotubes (**MW@N^{Az}**) have been conveniently prepared via [2+1] cycloaddition of *tert*-butyl-oxycarbonyl nitrene followed by a controlled thermal decomposition of the resulting carbamate. As a consequence of the outer material N-doping, the properties of pristine MWCNTs are deeply modified; surface microenvironments with specific base (Brønsted) and electronic features are formed. This translates into a highly versatile catalytic material with remarkable chemical and electrochemical performance. Indeed, the inclusion of NH groups in the Csp^2 network of MWCNTs translates into a redistribution of the charge density at the N-neighboring carbon sites. Such an electronic effect fosters the material oxygen adsorption properties and makes it a valuable electrocatalyst for promoting the kinetically sluggish oxygen reduction reaction (ORR). RRDE measurements under alkaline environment, demonstrate the efficiency of **MW@N^{Az}** as a metal-free system featured by a remarkable and positive shift of the overpotential values at which the ORR process starts (compared to pristine MWCNTs) along with a prevalent $4e^-$ reduction path. Finally, long-term cycling RRDE tests indicate the high resistance of the catalyst toward deactivation under operative conditions.

In addition, the basic character of the outer material surface widens the applicability range of this solid system in catalysis. Aziridine surface groups are then successfully engaged as basic sites for the Knoevenagel condensation in the presence of a variety of carbonyl compounds, showing superior

activities to those of related N-doped and N-decorated carbon nanomaterials of the *state-of-the-art*. Moreover, no appreciable decrease of chemical conversions is observed in the condensation process after multiple catalyst recovers and reuses (up to six times).

Despite a rather moderate N-loading ($\approx 1\%$ from EA), the adopted functionalization protocol for the grafting of basic groups makes them totally available at the outer material surface where the catalytic processes (ORR and Knoevenagel condensation) take place. The control of the surface N-groups finally offers a powerful tool for the rationalization and full exploitation of N-doped carbon nanomaterials as active systems in catalysis.

Acknowledgements

Thanks are due to the European FP7 project Freecats (contract n° NMP3-SL-2012-280658) for supporting this research activity.

Notes and References

- † Electronic Supplementary Information (ESI) available: TEM, recycling tests for the Knoevenagel condensation and electrochemical data processing for **MW@N^{Az}** sample. See DOI: 10.1039/x0xx00000x
1. D. S. Su, S. Perathoner and G. Centi, *Chem. Rev.*, 2013, **113**, 5782-5816.
 2. D. W. Wang and D. S. Su, *Energy Environ. Sci.*, 2014, **7**, 576-591.
 3. D. R. Dreyer and C. W. Bielawski, *Chem. Sci.*, 2011, **2**, 1233-1240.
 4. P. Serp and B. Machado *Nanostructured Carbon Materials for Catalysis*, The Royal Society of Chemistry, United Kingdom, Croydon, CR0 4YY, UK, 2015.
 5. K. Gong, F. Du, Z. Xia, M. Durstock and L. Dai, *Science*, 2009, **323**, 760-764.
 6. X. Wang, X. Li, L. Zhang, Y. Yoon, P. K. Weber, H. Wang, J. Guo and H. Dai, *Science*, 2009, **324**, 768-771.
 7. Y. Gao, G. Hu, J. Zhong, Z. Shi, Y. Zhu, D. S. Su, J. Wang, X. Bao and D. Ma, *Angew. Chem. Int. Ed.*, 2013, **52**, 2109-2113.
 8. Y. Deng, Y. Xie, K. Zou and X. Ji, *J. Mater. Chem. A*, 2016, **4**, 1144-1173.
 9. S. Majeed, J. Zhao, L. Zhang, S. Anjum, Z. Liu and G. Xu, *Nanotechnol. Rev.*, 2013, **2**, 615-635.
 10. X. Ge, A. Sumboja, D. Wu, T. An, B. Li, F. W. T. Goh, T. S. A. Hor, Y. Zong and Z. Liu, *ACS Catal.*, 2015, **5**, 4643-4667.
 11. G. Tuci, C. Zafferoni, P. D'Ambrosio, S. Caporali, M. Ceppatelli, A. Rossin, T. Tsoufis, M. Innocenti and G. Giambastiani, *ACS Catal.*, 2013, **3**, 2108-2111.
 12. G. Tuci, C. Zafferoni, A. Rossin, A. Milella, L. Luconi, M. Innocenti, L. Truong Phuoc, C. Duong-Viet, C. Pham-Huu and G. Giambastiani, *Chem. Mater.*, 2014, **26**, 3460-3470.

13. B. Kumar, M. Asadi, D. Pisasale, S. Sinha-Ray, B. A. Rosen, R. Haasch, J. Abiade, A. L. Yarin and A. Salehi-Khojin, *Nature Commun.*, 2013, **4**, 2819-2826.
14. X. Sun, X. Kang, Q. Zhu, J. Ma, G. Yang, Z. Liu and B. Han, *Chem. Sci.*, 2016, **7**, 2883-2887.
15. G. L. Tian, Q. Zhang, B. Zhang, Y.-G. Jin, J.-Q. Huang, D. S. Su and F. Wei, *Adv. Funct. Mater.*, 2014, **24**, 5956-5961.
16. C. A. Leon y Leon, J. M. Solar, V. Calemme and L. R. Radovic, *Carbon*, 1992, **30**, 797-811.
17. L. Zhang, J. Niu, L. Dai and Z. Xia, *Langmuir*, 2012, **28**, 7542-7550.
18. L. Lai, J. R. Potts, D. Zhan, L. Wang, C. K. Poh, C. Tang, H. Gong, Z. Shen, J. Lin and R. S. Ruoff, *Energy Environ. Sci.*, 2012, **5**, 7936-7942.
19. M. Kaukonen, R. Kujala and E. Kauppinen, *J. Phys. Chem. C*, 2012, **116**, 632-636.
20. G. Tuci, C. Zafferoni, A. Rossin, L. Luconi, A. Milella, M. Ceppatelli, M. Innocenti, Y. Liu, C. Pham-Huu and G. Giambastiani, *Catal. Sci. Technol.*, 2016, DOI: 10.1039/C6CY00796A.
21. E. Knoevenagel, *Chem. Ber.*, 1894, **27**, 2345-2346.
22. G. Jones, *Org. React.*, 1967, **15**, 204-599.
23. R. Menegatti, in *Green Chemistry – Aspects for the Knoevenagel Reaction*, eds. M. Kidwai and N. K. Mishra, 2012, DOI: DOI: 10.5772/36489, ch. 2.
24. S. van Dommele, K. P. De Jong and J. H. Bitter, *Chem. Commun.*, 2006, 4859-4861.
25. L. Wang, L. Wang, H. Jin and N. Bing, *Catal. Commun.*, 2011, **15**, 78-81.
26. J. Xu, K. Shen, B. Xue, Y.-X. Li and Y. Cao, *Catal. Lett.*, 2013, **143**, 600-609.
27. L. Zhang, H. Wang, Z. Qin, J. Wanga and W. Fan, *RSC Adv.*, 2015, **5**, 22838-22846.
28. J. Xu, K. Shen, B. Xue and Y.-X. Li, *J. Mol. Catal. A: Chem.*, 2013, **372**, 105-113.
29. F. Su, M. Antonietti and X. Wang, *Catal. Sci. Technol.*, 2012, **2**, 1005-1009.
30. J. Xu, Y. Wang, J.-K. Shang, Q. Jiang and Y.-X. Li, *Catal. Sci. Technol.*, 2016, **6**, 4192-4200.
31. J. Xu, T. Chen, Q. Jiang and Y.-X. Li, *Chem. Asian J.*, 2014, **9**, 3269-3277.
32. S. N. Talapaneni, S. Anandan, G. P. Mane, C. Anand, D. S. Dhawale, S. Varghese, A. Mano, T. Moric and A. Vinu, *J. Mater. Chem.*, 2012, **22**, 9831.
33. N. Kan-nari, S. Okamura, S.-i. Fujita, J.-i. Ozaki and M. Arai, *Adv. Synth. Catal.*, 2010, **352**, 1476-1484.
34. S.-i. Fujita, A. Katagiri, H. Watanabe, S. Asano, H. Yoshida and M. Arai, *ChemCatChem*, 2015, **7**, 2965-2970.
35. A. Yang, J. Li, C. Zhang, W. Zhang and N. Ma, *Appl. Surf. Sci.*, 2015, **346**, 443-450.
36. Y. Sun, C. Cao, P. Huang, S. Yang and W. Song, *RSC Adv.*, 2015, **5**, 86082-86087.
37. J. Xu, K.-Z. Long, T. Chen, B. Xue, Y.-X. Li and Y. Cao, *Catal. Sci. Technol.*, 2013, **3**, 3192-3199.
38. D. D. Perrin, W. L. F. Armarego and D. R. Perrin *Purification of Laboratory Chemicals*, Pergamon, New York, 2nd ed. edn., 1980.

39. L. A. Carpino, B. A. Carpino, P. J. Crowley, C. A. Giza and P. H. Terry, *Org. Synth.*, 1964, **44**, 15-17.
40. J. F. Moulder, W. F. Stickle, P. E. Sobol and K. D. Bomben J. C. (Ed.) *Handbook of X-ray Photoelectron Spectroscopy*, Perkin-Elmer Corporation, Minnesota, 1992.
41. B. Ballesteros, G. de la Torre, C. Ehli, G. M. Aminur Rahman, F. Agulló-Rueda, D. M. Guldi and T. Torres, *J. Am. Chem. Soc.*, 2007, **129**, 5061-5068.
42. E. Moaseri, M. Baniadam, M. Maghrebi and M. Karimi, *Chem. Phys. Lett.*, 2013, **555**, 164-167.
43. S. Treimer, A. Tang and D. C. Johnson, *Electroanalysis*, 2002, **14**, 165-171.
44. D. Tasis, N. Tagmatarchis, A. Bianco and M. Prato, *Chem. Rev.*, 2006, **106**, 1105-1136.
45. M. Holzinger, O. Vostrowsky, A. Hirsch, F. Hennrich, M. Kappes, R. Kappes and F. Jellen, *Angew. Chem. Int. Ed.*, 2001, **40**, 4002-4005.
46. M. Holzinger, J. Abraham, P. Whelan, R. Graupner, L. Ley, F. Hennrich, M. Kappes and A. Hirsch, *J. Am. Chem. Soc.*, 2003, **125**, 8566-8580.
47. C. Gao, H. He, L. Zhou, X. Zheng and Y. Zhang, *Chem. Mater.*, 2009, **21**, 360-370.
48. H. Leinonen, J. Rintala, A. Siitonen, M. Lajunen and M. Pettersson, *Carbon*, 2010, **48**, 2425-2434.
49. M. R. Banks, J. I. G. Cadogan, I. Gosney, P. K. G. Hodgson, P. R. R. Langridge-Smith, J. R. A. Millar and A. T. Taylor, *J. Chem. Soc., Chem. Commun.*, 1995, 885-886.
50. M. Quintana, K. Spyrou, M. Grzelczak, W. R. Browne, P. Rudolf and M. Prato, *ACS Nano*, 2010, **4**, 3527-3533.
51. M. M. Mahat, D. Mawad, G. W. Nelson, S. Fearn, R. G. Palgrave, D. J. Payne and M. M. Stevens, *J. Mater. Chem. C*, 2015, **3**, 7180-7186.
52. A. Goeppert, M. Czaun, G. K. S. Prakash and G. A. Olah, *Energy Environ. Sci.*, 2012, **5**, 7833-7853.
53. The authors are aware that any comparison of this type is technically difficult to be properly addressed due to the (always) different experimental conditions adopted in the literature for the catalytic runs (i.e. solvent, temperature and heating apparatus).
54. C. Song and J. Zhang, in *PEM Fuel Cell Electrocatalysts and Catalyst Layers: Fundamentals and Applications*, ed. J. Zhang, Springer, New York, 2008, pp. 89-134.
55. Y. Wang, D. Zhang and H. Liu, *J. Power Sources*, 2010, **195**, 3135-3139.
56. I. Kruusenberg, J. Leis, M. Arulepp and K. Tammeveski, *J. Solid State Electrochem.*, 2010, **14**, 1269-1277.
57. A. Morozan, P. Jégou, M. Pinault, S. Campidelli, B. Jousselme and S. Palacin, *ChemSusChem*, 2012, **5**, 647-651.
58. A. J. Bard and L. R. Faulkner I. John Wiley & Sons *Electrochemical Methods: Fundamentals and Applications*, 2nd edn., 2001.
59. Y. M. Tan, C. F. Xu, G. X. Chen, N. F. Zheng and Q. J. Xie, *Energy Environ. Sci.*, 2012, **5**, 6923-6927.
60. Y. Jiang, Y. Lu, X. Wang, Y. Bao, W. Chena and L. Niu, *Nanoscale*, 2014, **6**, 15066-15072.
61. D.-W. Kim, O. L. Liab and N. Saito, *Phys. Chem. Chem. Phys.*, 2015, **17**, 407-413.